Article

"Acid + Oxidant" Treatment Enables Selective Extraction of Lithium from Spent NCM523 Positive Electrode

Hui Wang [1], Zejia Wu [1], Mengmeng Wang [1], Ya-Jun Cheng [1], Jie Gao [1],* and Yonggao Xia [1,2],*

[1] Ningbo Institute of Materials Technology and Engineering, Chinese Academy of Sciences, 1219 Zhongguan West Road, Zhenhai District, Ningbo 315201, China; chengyj@nimte.ac.cn (Y.-J.C.)

[2] Center of Materials Science and Optoelectronics Engineering, University of Chinese Academy of Sciences, 19A Yuquan Rd, Shijingshan District, Beijing 100049, China

* Correspondence: gaojie@nimte.ac.cn (J.G.); xiayg@nimte.ac.cn (Y.X.)

Abstract: With the rapid development of new energy vehicles and energy storage industries, the demand for lithium-ion batteries has surged, and the number of spent LIBs has also increased. Therefore, a new method for lithium selective extraction from spent lithium-ion battery cathode materials is proposed, aiming at more efficient recovery of valuable metals. The acid + oxidant leaching system was proposed for spent ternary positive electrode materials, which can achieve the selective and efficient extraction of lithium. In this study, 0.1 mol L^{-1} H_2SO_4 and 0.2 mol L^{-1} $(NH_4)_2S_2O_8$ were used as leaching acid and oxidant. The leaching efficiencies of Li, Ni, Co, and Mn were 98.7, 30, 3.5, and 0.1%, respectively. The lithium solution was obtained by adjusting the pH of the solution. Thermodynamic and kinetic studies of the lithium leaching process revealed that the apparent activation energy of the lithium leaching process is 46 kJ mol^{-1} and the rate step is the chemical reaction process. The leaching residue can be used as a ternary precursor to prepare regenerated positive electrode materials by solid-phase sintering. Electrochemical tests of the regenerated material proved that the material has good electrochemical properties. The highest discharge capacity exceeds 150 mAh g^{-1} at 0.2 C, and the capacity retention rate after 100 cycles exceeds 90%. The proposed new method can extract lithium from the ternary material with high selectivity and high efficiency, reducing its loss in the lengthy process. Lithium replenishment of the delithiation material can also restore its activity and realize the comprehensive utilization of elements such as nickel, cobalt, and manganese. The method combines the lithium recovery process and the material preparation process, simplifying the process and saving costs, thus providing new ideas for future method development.

Keywords: spent lithium-ion batteries; positive electrode; recycling; acid; oxidation; selective extraction of lithium

1. Introduction

Lithium-ion batteries (LIBs) [1–3] have been widely used in 3C electronics, energy storage, and new energy electric vehicles due to their high energy density, long cycle life, low self-discharge, and superior safety performance [4–8] over other types of rechargeable batteries. The rapid development of new energy vehicles in recent years has led to a huge demand for lithium-ion batteries [9–12]. According to the statistics released by SNE research, the total installed capacity of global power batteries will be as high as 705.5 GWh in 2023, while the life span of lithium-ion batteries is only 5–8 years, which means that many LIBs will face retirement. Spent LIBs contain not only many harmful substances (such as electrolytes), but also many valuable metals (Li, Ni, Co, etc.), which may pollute soil, air, and water and waste resources if they are not properly treated. Therefore, lithium-ion battery recycling is of great significance, both at the level of environmental protection and at the economic level [7].

Currently, the main methods for recycling used lithium-ion batteries include mechanochemical [13,14], thermochemical [15–17], and hydrometallurgical methods. The mechanochemical method consists of a simple process, but it is mostly used in scientific research and is more difficult to apply in production. The pyrochemical method includes high-temperature melting and positive electrode material roasting. Among them, the high-temperature melting method is more used in industry due to the simple and efficient process. The battery does not need to be disassembled and is directly treated at a high temperature in a melting furnace to obtain the metal alloy. Due to the different boiling points of each metal, the low-boiling-point metal will be wrapped by the furnace gas and then condensed and collected to achieve the separation of each metal element. The method requires a high temperature, generally around 1000 °C, and therefore generates high energy consumption and waste gas pollution during the process. In addition, the low efficiency of lithium recovery is also a major drawback of this method. The positive electrode material roasting method is a more investigated for recycling spent LIBs. In general, the positive electrode material roasting method requires a lower temperature and consumes less energy compared to the high-temperature melting method. For the ternary positive electrode material, the waste battery is generally disassembled and sorted to obtain the positive electrode powder, which is roasted with reducing substances or under a reducing atmosphere to destroy the layered structure and reduce the high-valent transition metals to achieve the recovery of valuable metal resources [18,19]. Liu et al. [20] mixed the spent ternary materials and carbon black, then calcined it at 550 °C for 0.5 h prior to water leaching at room temperature. This enabled the preferential extraction of lithium from the spent ternary positive electrode material, and the nickel–cobalt–manganese oxide was obtained by acid leaching followed by gradual separation of high-purity nickel, cobalt, and manganese compounds. The process can achieve a lithium leaching efficiency of 93.68% and nickel, cobalt, and manganese leaching efficiency of more than 99%.

The hydrometallurgical method mainly uses mineral acid (hydrochloric acid [21], sulfuric acid [22], nitric acid [23]) to leach the positive electrode material, and then achieves step-by-step extraction of each valent metal through certain processes. The process of the hydrometallurgical method is complex, but it has received much attention due to the advantages of obtaining products with higher purity and lower requirements for equipment, etc. Since the use of inorganic acids generates a large amount of wastewater, the use of organic acids such as acetic acid [24,25], ascorbic acid [26,27], and citric acid [28,29] as leaching acids has been increasingly reported in recent years. He et al. [30] used L-tartaric acid and hydrogen peroxide as leaching systems and were able to achieve leaching efficiencies of 99.07, 99.31, 98.64, and 99.31% for lithium, nickel, cobalt, and manganese, respectively. These results indicate that the use of organic acids can eliminate secondary contamination without sacrificing high leaching efficiency.

Valuable metals in positive electrode materials do not leach well in pure acids (without redox agent) and generally need to be used with redox agents. Wang et al. [31] used sulfuric acid and sodium thiosulfate as leaching systems to recover lithium-ion batteries and were able to achieve leaching efficiencies of 99.71 and 99.95% for lithium and cobalt, respectively. In this system, sodium persulfate is used as a reducing agent to lower the transition metal valence and allow for better leaching into solution. Industrial production generally uses a sulfuric acid and hydrogen peroxide leaching system to achieve the full component leaching of all metals (Li, Ni, Co, Mn, etc.) in ternary materials, and then the separation of each element by extraction or precipitation. However, lithium is generally recovered last in the process of separation and purification, and the yield is low.

Therefore, we propose an "acid + oxidant" leaching system to recover ternary lithium-ion batteries, which can achieve the selective and preferential extraction of lithium and avoid the problem of loss in the lengthy operation process. In addition, the transition metals can be used comprehensively. This method provides a new idea for the recovery and comprehensive utilization of spent LIB resources.

2. Experimental Section

2.1. Materials and Reagents

Spent LIBs were kindly supplied by RONBAY TECHNOLOGY (Ningbo, China). Carbon dioxide was purchased from Ningbo Wanli Gas Co. (Ningbo, China). Sulfuric acid was acquired from Tianqi Chemical Reagent Co., Ltd. (Shanghai, China). Ammonium persulfate was acquired from Aladdin Reagent Co., Ltd. (Shanghai, China). Carbon black (Super P, 99%) and NMP (N-methyl pyrrolidone, 99.5%) were acquired from Alfa Aesar (Shanghai, China) Chemical Co., Ltd. PVDF (poly (vinylidene difluoride), HSV900) was purchased from Arkema (Beijing, China) Co., Ltd. The electrolyte, supplied by Mitsui Chemicals (Tokyo, Japan), was 1.0 mol of $LiPF_6$ in a volume ratio of EC/DMC = 3:7.

2.2. Experimental Procedure

The specific steps of the experiment were as follows:

In this experiment, the raw material was spent NCM523 powder, and the oxidation acid leaching solution was 0.1 mol L^{-1} sulfuric acid and 0.2 mol L^{-1} ammonium persulfate. Spent NCM523 powder was added into the leaching solution with a solid–liquid ratio of 10–50 g L^{-1}, a reaction temperature of 30–90 °C, a magnetic stirring speed of 500 rpm, and a reaction time of 2–12 h.

We added alkali to the oxidation acid leached slurry, adjusted the pH of the solution to 11, and continued with magnetic stirring for 2 h. The filtrate obtained by filtration was the lithium solution, and the residue was the solid containing Ni-Co-Mn.

The solid obtained in the previous step was dried and mixed with $LiOH \cdot H_2O$. The mixed powder was calcined with a heating rate of 3 °C min^{-1}, heated to 800 °C, held for 10 h, and then cooled naturally. And PVDF was dissolved in NMP with the mass ratio of PVDF:NMP of 1:25. The mass compositions of the electrodes regarding the NCM811, Super-P, and PVDF were set as 8:1:1. The conductive carbon (Super P) and the prepared PVDF-NMP solution were mixed well in a high-speed homogenizer to obtain a uniform and stable positive electrode slurry. The mixing program was set to stir for 60, 180, and 60 s at 800, 1500, and 800 rpm, respectively. The positive electrode slurry was cast on aluminum foil and dried in a vacuum oven at 110 °C for 12 h.

To prepare the 2032-type half-cells, the dried positive electrodes were first cut into circular sheets 14 mm in diameter (with a mass loading of approximately 4.5 mg cm^{-2}), which were then combined with PP-PE-PP diaphragms (Celgard 825), a lithium foil counter electrode, gaskets, shrapnel, and the electrolyte (80 μL) to form the cells. After resting for 12 h, the cells were tested on the LAND Battery Test System (Wuhan, China). The charge/discharge tests had a voltage range of 2.8–4.3 V.

2.3. Analytical Methods

In this work, the metallic ion concentrations were tested using an inductively coupled plasma optical emission spectrometer (ICP-OES Varian 720ES, Palo Alto, CA, USA). The morphologies of the solid samples were characterized by environmental scanning electron microscopy (SEM Hitachi S4800, Tokyo, Japan) and a transmission electron microscope (TEM, Tecnai F20, FEI Company, Hillsboro, OR, USA). X-ray diffraction patterns were obtained using a powder diffractometer (XRD, D8 ADVANCE, BRUKER AXS, Billerica, MA, USA, equipped with Cu K_α radiation = 1.5406 Å, 2.2 kW, scanning rate: 0.02° s^{-1}, 2 θ ranges: 10–90°). The valences of Ni, Co, and Mn were characterized by X-ray photoelectron spectroscopy (XPS, Thermo Fisher Escalab 250XI, Waltham, MA, USA).

3. Results and Discussion
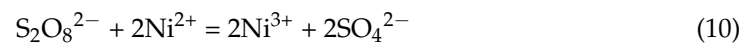
3.1. Analysis of Oxidation Acid Leaching Process

3.1.1. Thermodynamic Analysis of Oxidation Acid Leaching Process

To illustrate the feasibility of the oxidation acid leaching system, a thermodynamic analysis of the process was performed. The electrode potential indicates the oxidizing capacity of the oxidizing agent and the reducing capacity of the reducing substance, which

determines whether the redox reaction can proceed and the order in which the reaction proceeds. The following are the half-reactions of the ions involved in the oxidation-acid leaching process and their electrode potentials in the standard state.
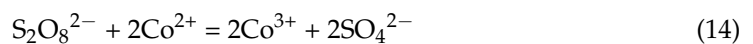
$$S_2O_8^{2-} + 2e = 2SO_4^{2-} \qquad E_1^{\theta} = 2.010 \text{ V} \qquad (1)$$

$$Ni^{3+} + e = Ni^{2+} \qquad E_2^{\theta} = 1.840 \text{ V} \qquad (2)$$

$$NiO_2 + 4H^+ + 2e = Ni^{2+} + 2H_2O \qquad E_3^{\theta} = 1.678 \text{ V} \qquad (3)$$

$$Co^{3+} + e = Co^{2+} \qquad E_4^{\theta} = 1.920 \text{ V} \qquad (4)$$

$$[Co(NH_3)_6]^{3+} + e = [Co(NH_3)_6]^{2+} \qquad E_5^{\theta} = 0.108 \text{ V} \qquad (5)$$

$$Mn^{3+} + e = Mn^{2+} \qquad E_6^{\theta} = 1.542 \text{ V} \qquad (6)$$

$$MnO_2 + 4H^+ + 2e = Mn^{2+} + 2H_2O \qquad E_7^{\theta} = 1.224 \text{ V} \qquad (7)$$

$$MnO_4^- + 8H^+ + 5e = Mn^{2+} + 4H_2O \qquad E_8^{\theta} = 1.507 \text{ V} \qquad (8)$$

$$NiO_2 + 2e + 2H_2O = Ni(OH)_2 + 2HO^- \qquad E_9^{\theta} = 0.490 \text{ V} \qquad (9)$$

The electrode potential difference ΔE between the oxidizing agent and the reducing agent reflects the driving force of the chemical reaction. If the electrode potential difference ΔE is larger, it indicates that the reaction driving force is larger. The standard electrode potential difference ΔE^{θ} for the oxidation of Ni^{2+}, Co^{2+}, $[Co(NH_3)_6]^{2+}$, Mn^{2+}, $Ni(OH)_2$ by $S_2O_8^{2-}$ in the oxidation acid leaching system and all possible reaction equations are shown below:
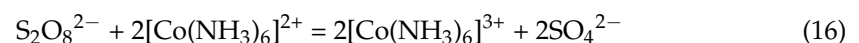
$$S_2O_8^{2-} + 2Ni^{2+} = 2Ni^{3+} + 2SO_4^{2-} \qquad (10)$$

$$\Delta E_1^{\theta} = E_1^{\theta} - E_2^{\theta} = 2.010 \text{ V} - 1.840 \text{ V} = 0.170 \text{ V} \qquad (11)$$

$$S_2O_8^{2-} + Ni^{2+} + 2H_2O = NiO_2 + 2SO_4^{2-} + 4H^+ \qquad (12)$$

$$\Delta E_2^{\theta} = E_1^{\theta} - E_3^{\theta} = 2.010 \text{ V} - 1.678 \text{ V} = 0.332 \text{ V} \qquad (13)$$

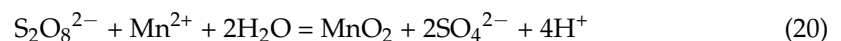$$S_2O_8^{2-} + 2Co^{2+} = 2Co^{3+} + 2SO_4^{2-} \qquad (14)$$

$$\Delta E_3^{\theta} = E_1^{\theta} - E_4^{\theta} = 2.010 \text{ V} - 1.920 \text{ V} = 0.090 \text{ V} \qquad (15)$$

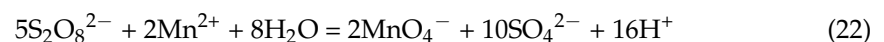$$S_2O_8^{2-} + 2[Co(NH_3)_6]^{2+} = 2[Co(NH_3)_6]^{3+} + 2SO_4^{2-} \qquad (16)$$

$$\Delta E_4^{\theta} = E_1^{\theta} - E_5^{\theta} = 2.010 \text{ V} - 0.108 \text{ V} = 1.902 \text{ V} \qquad (17)$$

$$S_2O_8^{2-} + 2Mn^{2+} = 2Mn^{3+} + 2SO_4^{2-} \qquad (18)$$

$$\Delta E_5^{\theta} = E_1^{\theta} - E_6^{\theta} = 2.010 \text{ V} - 1.542 \text{ V} = 0.468 \text{ V} \qquad (19)$$

$$S_2O_8^{2-} + Mn^{2+} + 2H_2O = MnO_2 + 2SO_4^{2-} + 4H^+ \qquad (20)$$

$$\Delta E_6^{\theta} = E_1^{\theta} - E_7^{\theta} = 2.010 \text{ V} - 1.224 \text{ V} = 0.786 \text{ V} \qquad (21)$$

$$5S_2O_8^{2-} + 2Mn^{2+} + 8H_2O = 2MnO_4^- + 10SO_4^{2-} + 16H^+ \qquad (22)$$

$$\Delta E_7^{\theta} = E_1^{\theta} - E_8^{\theta} = 2.010 \text{ V} - 1.507 \text{ V} = 0.503 \text{ V} \qquad (23)$$

The order of the above standard electrode potential difference is $\Delta E_4^{\theta} > \Delta E_6^{\theta} > \Delta E_7^{\theta} > \Delta E_5^{\theta} > \Delta E_2^{\theta} > \Delta E_1^{\theta} > \Delta E_3^{\theta}$. The smallest ΔE_3^{θ} represents the oxidation of Co^{2+} to Co^{3+} by $S_2O_8^{2-}$. But due to the presence of NH_4^+, the oxidation of Co^{2+} to Co^{3+} is transformed into the oxidation of $[Co(NH_3)_6]^{2+}$ to $[Co(NH_3)_6]^{3+}$, the standard electrode potential difference of the process is 1.902 V, and the reaction driving force is maximum. ΔE_2^{θ} and ΔE_1^{θ} are the smallest, all of which are the Ni^{2+} being oxidized, indicating that the driving force for the oxidation process of Ni^{2+} is minimal. Therefore, in the subsequent oxidation acid leaching experiment, some Ni^{2+} was found to be leached into the solution, which is also consistent with the theory. The above theoretical analysis proves that $S_2O_8^{2-}$ can not only maintain the oxidation leaching environment as strongly oxidizing agent, but

also oxidize the low-valent ions such as Ni^{2+}, Co^{2+}, $[Co(NH_3)_6]^{2+}$, and Mn^{2+} dissolved in the leaching solution to high-valent insoluble substances, so as to realize the selective and efficient leaching of lithium from spent ternary positive electrode materials.

In the oxidation acid leaching slurry with alkali precipitation of Ni^{2+}, the NaOH addition product should be $Ni(OH)_2$, while the XRD Figure 5a shows that the reaction product is NiO_2. From Equations (1) and (9), NiO_2 is generated by the oxidation of $Ni(OH)_2$ by $S_2O_8{}^{2-}$, and the standard potential difference of this process is ΔE^θ = 1.52 V, which has a large reaction driving force.

3.1.2. Dynamics Analysis of Oxidation Acid Leaching Process

In order to gain an in-depth understanding of the whole oxidation acid leaching process, the study of the kinetics of the leaching of valuable metals is essential. The leaching of valuable metals is the process of moving metal ions from a solid metal oxide into the liquid phase. The leaching reaction process proceeds from the outer surface of the particle toward the inner core, and the particle slowly shrinks until the reaction is completed. This process is a combination of mass transfer, diffusion, and chemical reaction. Originally used to analyze the kinetics of crystallization processes and later applied to describe the kinetics of leaching reactions for various minerals, the Avrami equation model will be introduced in this section to describe the leaching kinetics of positive electrode materials for decommissioned lithium-ion batteries. We understand the reaction mechanism of the whole oxidation acid leaching process from the leaching kinetics. The role of the oxidizing agent in this leaching system is to inhibit the leaching of manganese and cobalt, and their leaching efficiencies are too low to study their leaching kinetics. Some nickel elements in the spent ternary material will enter the leaching solution, but the process involves redox reactions in addition to acid leaching, and its leaching kinetics cannot be studied singularly. Therefore, we only study the leaching kinetics of lithium in spent ternary materials. The reaction rate control steps are usually surface chemical reaction control (Equation (24)), diffusion control (Equation (25)), logarithmic rate control (Equation (26)), and the Avrami equation (Equation (27)).

$$1 - (1 - x)^{1/3} = k_1 t \tag{24}$$

$$1 - (2/3)\,x - (1 - x)^{2/3} = k_2 t \tag{25}$$

$$(-\ln(1 - x))^2 = k_3 t \tag{26}$$

$$\ln(-\ln(1 - x)) = \ln k_4 + n \ln t \tag{27}$$

where x is the fraction of the reaction, k_1 to k_4 are the reaction rate constants (h^{-1}), t is the leaching time (h), and n is determined by the fitting results.

The apparent activation energy (E_a) of the valent metal represents the difficulty of the reaction and can be determined from the Arrhenius equation as follows:

$$\ln k = \ln A - E_a / RT \tag{28}$$

where k is the reaction rate constant (h^{-1}), E_a is the surface activation energy (kJ mol^{-1}), and T is the absolute temperature (K).

It can be seen from the above equation (Equation (28)) that $\ln k$ and $1/T$ are linearly related, and the apparent activation energy of metal leaching can be found by plotting $\ln k$ and $1/T$ with a slope of $-E_a/R$.

The kinetics of lithium leaching from spent ternary materials were studied with different reaction times (0–9 h) and temperatures (20–65 °C). Other conditions were controlled at the optimum level, and the leaching data were substituted into the four models (Equations (20)–(23)) with t or $\ln t$ as the horizontal coordinates and $(-\ln(1 - x))^2$, $1 - (2/3)x - (1 - x)^{2/3}$, $(1 - x)^{1/3}$, $\ln(-\ln(1 - x))$ as the vertical coordinates for the graphs, respectively, to obtain the kinetic equations of lithium leaching. The results are shown in Figure 1. The specific parameters of the fitting are in Table 1, where the value of R^2 reflects the degree of fitting.
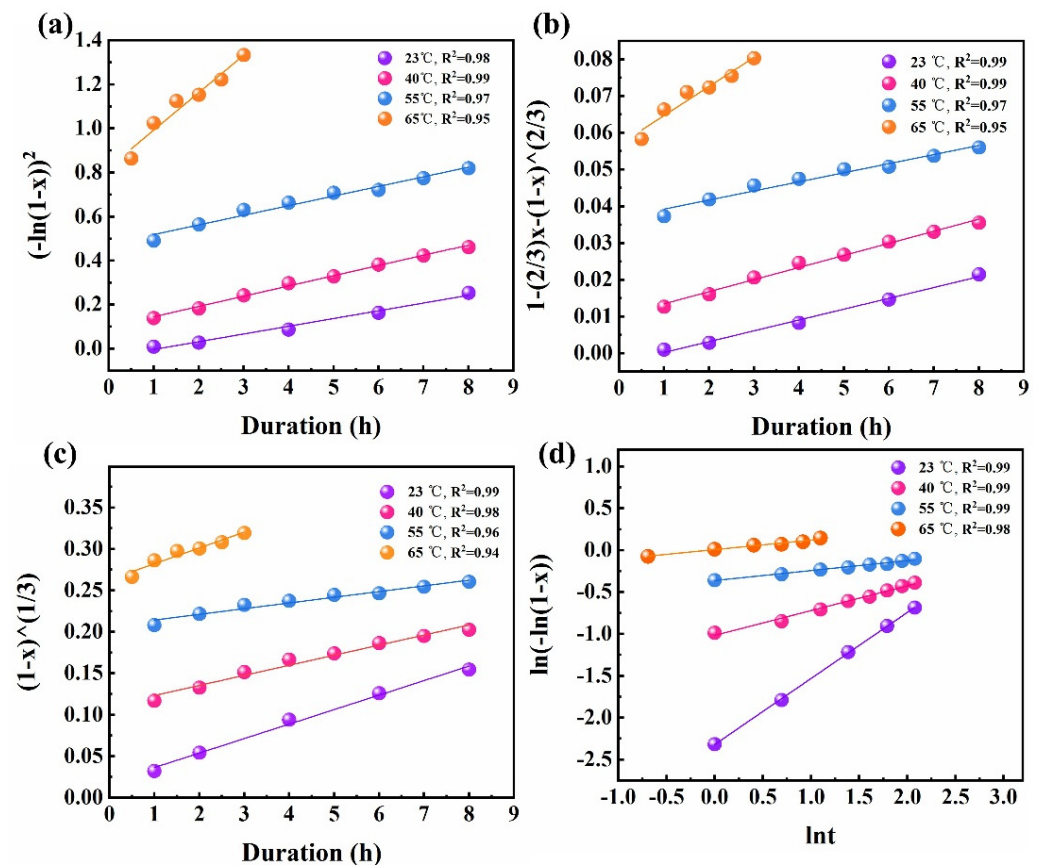
Figure 1. Simulation of lithium leaching kinetics during oxidation acid leaching. (**a**) Logarithmic rate control model, (**b**) diffusion control model, (**c**) chemical reaction control model, (**d**) Avrami equation model.

Table 1. Fitting degrees for the four models.

Fitting Model	Temperature (°C)	lnk	R^2
Logarithmic rate model	23	/	0.9855
	40	/	0.9953
	55	/	0.9744
	65	/	0.9542
Diffusion control model	23	/	0.9935
	40	/	0.9905
	55	/	0.9676
	65	/	0.9453
Chemical reaction control model	23	/	0.9935
	40	/	0.9766
	55	/	0.960
	65	/	0.939
Avrami equation model	23	−2.319	0.999
	40	−1.016	0.989
	55	−0.362	0.987
	65	0.006	0.981

It can be seen from Figure 1a–c and Table 1 that the chemical reaction control model and the internal diffusion control model have poor correlation fits, while the Avrami equation model ($R^2 > 0.98$) has a better fit correlation compared to the other models. The Avrami equation model has the best fitting correlation, indicating that the kinetics is mainly controlled by the inverse process of the crystal. This also demonstrates that the Avrami equation can be used to explain the leaching of solids containing multiple metallic elements

in the liquid phase system. The fits of the other models are good at low temperatures, but decrease as the temperature increases. The intercept of the Avrami equation is ln*k*, and from the fitting results, Table 1 shows that the intercept increases sequentially from a low to a high temperature, indicating that the reaction rate constant increases with increasing temperature. This also indicates that increasing the reaction temperature is beneficial to leaching.

A plot of ln*k* versus $1/T$ was obtained by fitting the temperature and rate constants from the Avrami equation model, as shown in Figure 2. The slope of the straight line is $-E_a/R$. $R^2 = 0.98$ indicates that the fit is very good. The apparent activation energy of Li leaching in the leaching system can be calculated to be 46 kJ/mol, indicating that the reaction rate in the leaching process is controlled by the surface chemistry.
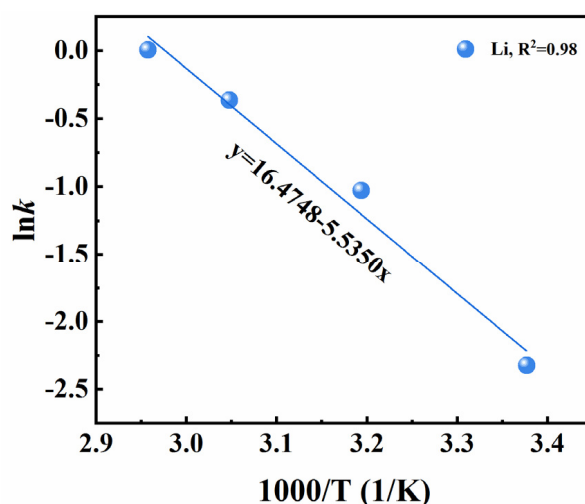
Figure 2. Arrhenius plots for leaching of Li from the positive electrode scrap.

3.1.3. Optimization of Oxidation Acid Leaching Reaction Conditions

The concentrations of the oxidizer and acid, as well as the reaction time, temperature, and solid–liquid ratio, all have effects on the leaching efficiency of valuable metal ions. In order to understand the whole process, it is necessary to conduct single-factor experiments on the leaching process, and the results are shown in Figure 3.

The effects of sulfuric acid concentration on the leaching efficiency of metals such as lithium, nickel, cobalt, and manganese were studied. The role of acid in this leaching system is to destroy the structure of the waste material and to leach the lithium from the material into the leaching solution. The leaching of other elements cannot be avoided in this process. It can be seen from Figure 3a that the leaching efficiencies of Li, Ni, and Co all increased with increasing acid concentration, and the change in Mn leaching efficiency was not obvious. When the sulfuric acid concentration was 1 mol L^{-1}, the leaching efficiency effect of lithium was excellent, reaching 99.6%, but the leaching efficiency of nickel and cobalt also reached about 50%, and the effect of lithium selective extraction could not be achieved. When the acid concentration was 0.1 mol L^{-1}, the lithium leaching efficiency reached 97.2%; the manganese leaching efficiency was extremely low; the cobalt leaching efficiency was below 10%; and the nickel leaching efficiency was at a relatively low level, 28%. The leaching efficiencies of cobalt and nickel increased when the concentration of acid increased, while the leaching efficiency of lithium decreased when the concentration of acid decreased. Therefore, a 0.1 mol L^{-1} acid concentration was chosen as the optimum acid concentration.
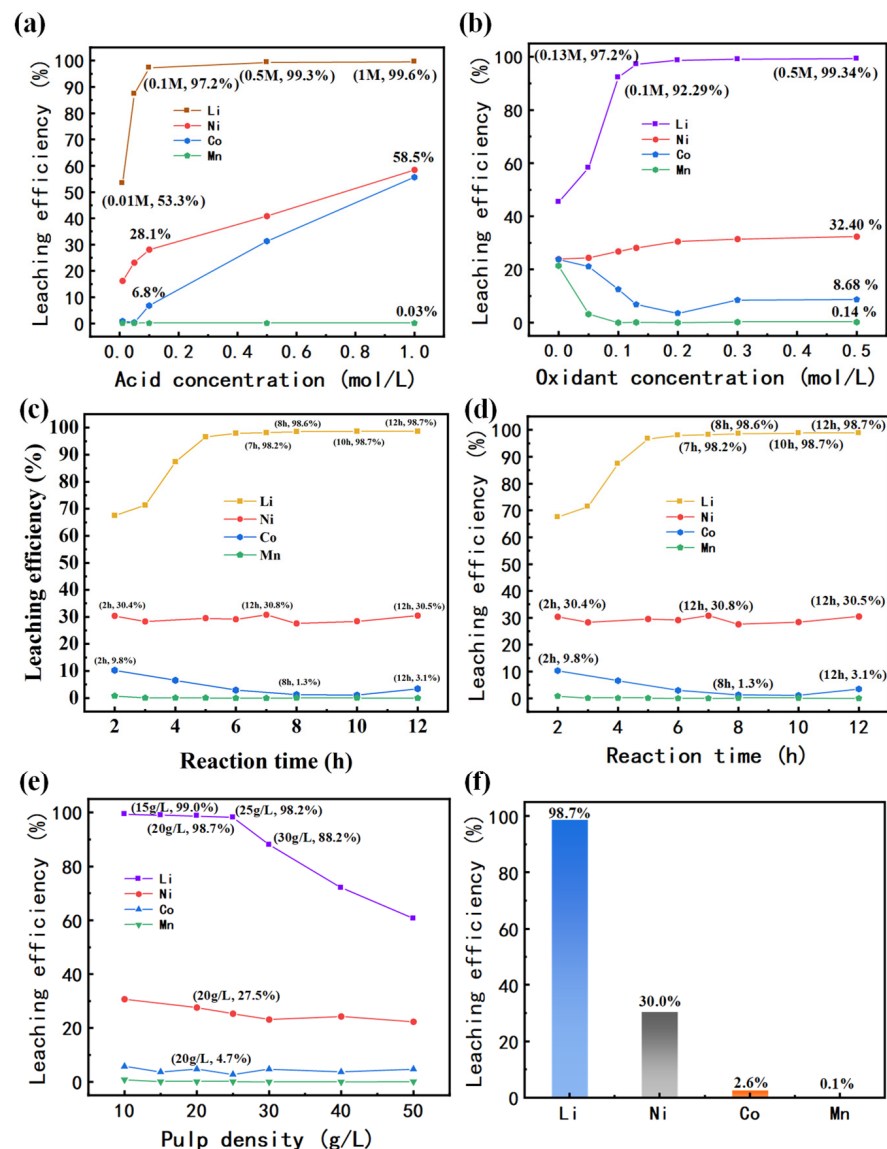
Figure 3. The relationship between the leaching efficiency of metal elements and (**a**) acid concentration, (**b**) oxidant concentration, (**c**) reaction time, (**d**) reaction temperature, (**e**) pulp density, and (**f**) leaching efficiency of each element under optimal conditions.

The effects of different oxidant concentrations on the leaching efficiency of lithium, nickel, cobalt and manganese metals was investigated. The role of the oxidant in this leaching system was to inhibit the leaching of transition metal elements. Sulfuric acid leaching is not selective, and the addition of the oxidant reduces the leaching of transition metal elements so that the lithium in the spent ternary materials can be leached selectively. Firstly, only 0.1 mol L^{-1} sulfuric acid was used to leach the spent ternary materials, and it was found that the leaching under this condition was not selective. The leaching efficiency of lithium was less than 50%, and the leaching efficiencies of nickel, cobalt, and manganese also reached more than 20%. As the concentration of oxidant increased, the leaching efficiency of lithium increased rapidly, the leaching efficiency of nickel increased slowly, and the leaching efficiencies of cobalt and manganese decreased. This indicates that the high concentration of ammonium persulfate can inhibit the leaching of cobalt and manganese and slow down the leaching of nickel, but not at a lower level. There was a slight increase after the decrease of cobalt leaching efficiency, as shown in Figure 3b, which we believe was due to an error during the experiment because the temperature could not be kept the same for each group of experiments. When the oxidant concentration was 0.2 mol L^{-1}, 98.7%

of the lithium in the spent ternary material could be leached into the leaching solution, and the leaching efficiencies of cobalt, nickel, and manganese were maintained at a low level. When the oxidant concentration was less than 0.2 mol L^{-1}, the lithium leaching efficiency could not reach the requirement, and the cobalt leaching efficiency was also relatively high. When the oxidant concentration was greater than 0.2 mol L^{-1}, the leaching of lithium, nickel, cobalt, and manganese did not change much. Thus, the optimal oxidant concentration was chosen to be 0.2 mol L^{-1}.

The effects of different reaction times on the leaching efficiencies of metals such as lithium, nickel, cobalt, and manganese were investigated. Since the leaching system used a low concentration of acid, which has a limited ability to damage the structure of the material, longer reaction times were required. The reaction times were controlled at 2–12 h. It can be seen from Figure 3c that the length of the reaction time had little effect on the leaching of nickel, cobalt and manganese elements, while the leaching efficiency of lithium became higher as the reaction time increased. The lithium leaching efficiencies were 96.6% at the reaction time of 5 h, 98.0% at the reaction time of 6 h, and 98.2% at the reaction time of 7 h. The lithium leaching efficiency was low when the reaction times were 5 h and below, and when the reaction times were 7 h and above, the lithium leaching efficiency was maintained at a high level with little variation, so 6 h was chosen as the optimal reaction time to ensure high lithium leaching efficiency and high selectivity, as well as to relatively reduce the heating energy and time costs.

The effects of different reaction temperatures on the leaching efficiencies of lithium, nickel, cobalt, and manganese metals were investigated. The reaction temperature was controlled at 25–95 °C, and graphs of the variation in the leaching efficiency of lithium, nickel, cobalt, and manganese at different reaction temperatures were obtained (Figure 3d). As shown in Figure 3d, the lithium leaching efficiency was low at a low temperature, and there was no selectivity. The leaching efficiency of lithium increased rapidly with the increase in temperature. This may have been due to the enhanced mass transfer effect of increasing temperature, which led to faster leaching of lithium. When the temperature was 60–70 °C, the leaching efficiencies of cobalt and manganese decreased rapidly. This indicates that the oxidation leaching system had no or a weak inhibitory effect on the leaching of transition metal elements at a low temperature, and the inhibitory effect increased with the increase in temperature. When the temperature increased to a certain degree, the leaching efficiency of transition metal elements could be limited to a low level (less than 10%), and the leaching of lithium had a certain selectivity. When the temperature was lower than 65 °C, the lithium leaching efficiency was lower than 92%, the cobalt and manganese leaching efficiencies were larger, and the lithium selectivity was smaller. When the temperature was 65 °C, the lithium leaching efficiency reached 98.7%, while the cobalt and manganese leaching efficiencies were lower than 5%, and the lithium leaching selectivity was higher. When the temperature was higher than 65 °C, the lithium and cobalt and manganese leaching efficiencies did not change much, but the nickel leaching efficiency continued to grow. Therefore, the optimum reaction temperature of 65 °C was determined to ensure high lithium leaching efficiency and high selectivity, and also to relatively reduce heating energy consumption.

The effect of different solid–liquid ratios on the leaching efficiencies of lithium, nickel, cobalt, and manganese metals was investigated. A larger solid–liquid ratio allowed for a higher concentration of lithium solution in the leachate, reducing the cost of the concentration process and facilitating the preparation of lithium carbonate at a later stage. However, it can be seen from Figure 3e that the lithium leaching decreased when the solid–liquid ratio increases. Therefore, a suitable solid–liquid ratio was necessary to achieve both high lithium leaching efficiency and high selectivity. As shown in Figure 3e, the leaching efficiencies of lithium, nickel, cobalt, and manganese were 98.2, 25.3, 2.7, and 0.03%, respectively, when the solid–liquid ratio was 25 g L^{-1}. When the solid–liquid ratio was less than 25 g L^{-1}, the lithium leaching efficiency and selectivity were also at a high level, but the low solid–liquid ratio meant that the concentration of lithium ions in the

leachate was low, increasing the evaporation concentration cost. When the solid–liquid ratio was greater than 25 g L^{-1}, the lithium leaching efficiency decreased rapidly. Therefore, the solid–liquid ratio of 25 g L^{-1} charging was chosen as the best solid–liquid ratio for the reaction, ensuring a high Li^+ concentration in the leachate, but also a high lithium leaching efficiency and good selectivity.

It can be concluded from the above series of experiments that the optimal reaction conditions for this reaction are $c[H_2SO_4] = 0.1$ mol L^{-1}, $c[(NH_4)_2S_2O_8] = 0.2$ mol L^{-1}, $t = 6$ h, $T = 65\ °C$, and a dosing solid–liquid ratio of 25 g L^{-1}. The experimental leaching efficiencies of Li, Ni, Co, and Mn under these conditions were 98.7, 30.0, 3.5, and 0.1%, as shown in Figure 3f. The lithium leaching efficiency was at a high level, while the leaching efficiencies of both cobalt and manganese were low, indicating that the lithium leaching selectivity was good. Then, by adding sodium hydroxide to the leaching solution to precipitate Ni^{2+}, a pure lithium solution was obtained for the preparation of Li_2CO_3.

3.1.4. Physical Phase Analysis of Oxidation Acid Leaching Process

The SEM images of the raw spent ternary positive electrode material, the direct filtration slag after oxidation acid leaching, and the precipitation slag after oxidation acid leaching with sodium hydroxide are shown in Figure 4. It can be seen from Figure 4a–c that the particles of the spent ternary positive electrode material were broken, irregular in shape, and agglomerated. It can be observed in Figure 4d–f that, after oxidation acid leaching, the surface of the particles became smooth, and the agglomerated large particles were dispersed and had a certain sphericity. The oxidation acid leaching treatment was followed by adding sodium hydroxide to the beaker to adjust the pH of the solution so that the nickel ions and OH^- in the solution combined to form the precipitate. The resulting mixed slag contained nickel hydroxide and the ternary materials of delithiation, and their SEM images are shown in Figure 4g–i. Due to the treatment of strong alkali, the surface of the material was not so smooth, and the particle shape was irregular. The leached nickel ions were precipitated by adding sodium hydroxide to the leaching slurry to adjust the pH, and a solid slag was obtained after the reaction was completed, which was used as a precursor for the ternary material. The precursor and lithium source (lithium hydroxide monohydrate) were mixed thoroughly with a ball mill and calcined under an oxygen atmosphere to prepare the regenerated ternary positive electrode material (R-NCM523). The SEM images of the regenerated material are shown in Figure 4a–c, and they show a smoother particle surface, relatively more uniform particle size, and better sphericity compared to the oxidized leach slag.

The XRD patterns before and after the oxidation acid leaching are shown in Figure 5. Specifically, the black curve is the XRD pattern of the spent ternary positive electrode material (NCM523), the red curve is the XRD pattern of the solid slag obtained by direct filtration after the oxidation acid leaching, and the blue curve shows the XRD pattern of the leached slag obtained by adding NaOH to adjust the pH to 11 after the oxidation acid leaching. It can be observed that the XRD peak patterns and positions of the oxidation leaching slag and the spent ternary material are similar, indicating that the structure of the slag obtained from the oxidation acid leaching of NCM523 material did not change drastically, and only the lithium in the lamellar structure of the material was stripped out, maintaining the lamellar structure of NCM523, as shown in Figure 5b. The blue curve in Figure 5a shows only two peaks in the dashed box, more than the red curve. These two peaks represent the NiO_2 generated by the oxidation of Ni^{2+} through oxidation acid leaching during the process of alkali precipitation, and the PDF card below can be a good match. It is known from the thermodynamic analysis section that the standard electrode potential for $Ni(OH)_2$ to be oxidized to NiO_2 is 0.49 V, while the oxidation potential of $S_2O_8^{2-}$ is 2.01 V. The excess oxidant from the oxidation acid leaching process was sufficient to oxidize $Ni(OH)_2$ to NiO_2, and the theory is consistent with reality.
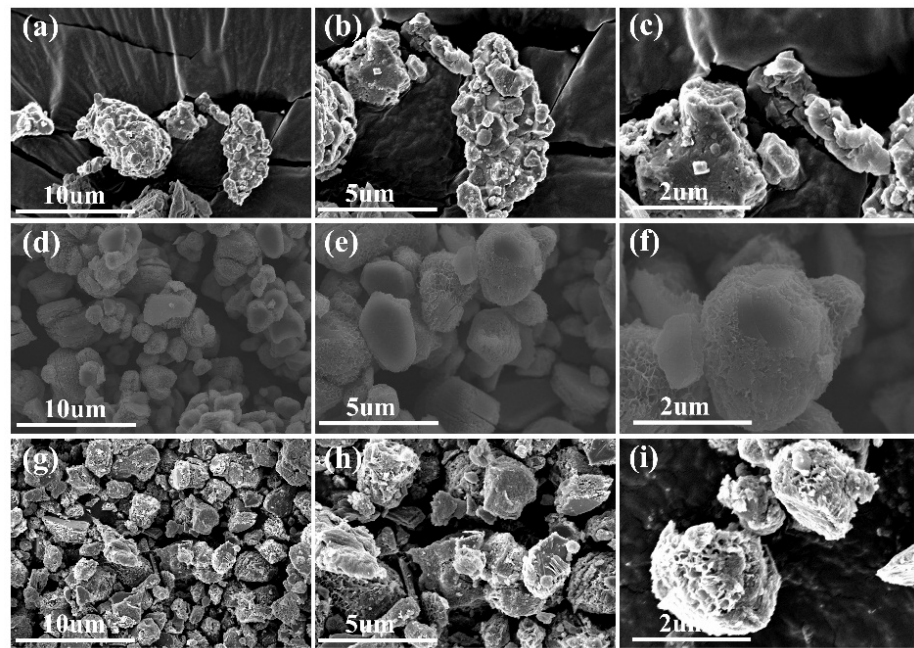
Figure 4. SEM images of (**a**–**c**) spent NCM523, (**d**–**f**) oxidation acid leaching residue without NaOH, (**g**–**i**) oxidation acid leaching residue with NaOH.
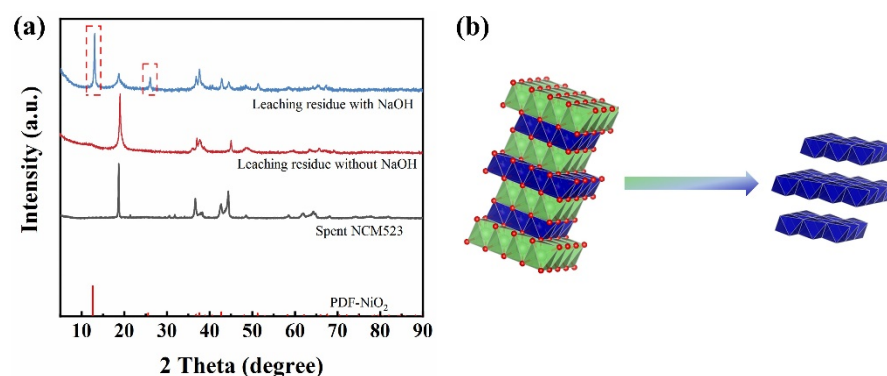

Figure 5. (**a**) XRD pattern of residues after and before oxidation acid leaching; (**b**) schematic diagram of oxidation acid leaching.

In addition, ICP-OES was used to test the Ni, Co, and Mn contents in the slag after oxidation acid leaching followed by NaOH precipitation, and Ni:Co:Mn = 5:2:3 (molar ratio) was obtained, which is consistent with our experimental concept and can be used for the preparation of regenerated positive electrode material (R-NCM523).

3.1.5. Analysis of the Mechanism of Oxidation Acid Leaching

The XPS spectra comparing the surface of the scrap NCM523 raw material and the oxidation acid leaching slag without alkali sink are shown in Figure 6. The XPS pattern of Ni 2p is shown in Figure 6a. The binding energy of the spent NCM523 material had two main peaks of Ni $2p^{3/2}$ and Ni $2p^{1/2}$ at 854.0 eV and 872.0 eV, and two satellite peaks with binding energies of 860.9 eV and 879.0 eV, which are close to the binding energy data of Ni^{2+} [32,33]. The two strong peaks at binding energies of 855.5 eV and 873.1 eV prove the presence of Ni^{3+}. The peaks of Ni^{2+} disappeared from the XPS spectrum of the powder after the oxidation acid leaching treatment, and only the peaks of Ni^{3+} remained, indicating that after oxidation acid leaching treatment, some Ni^{2+} leached into the solution and some Ni^{2+} was oxidized to Ni^{3+}.
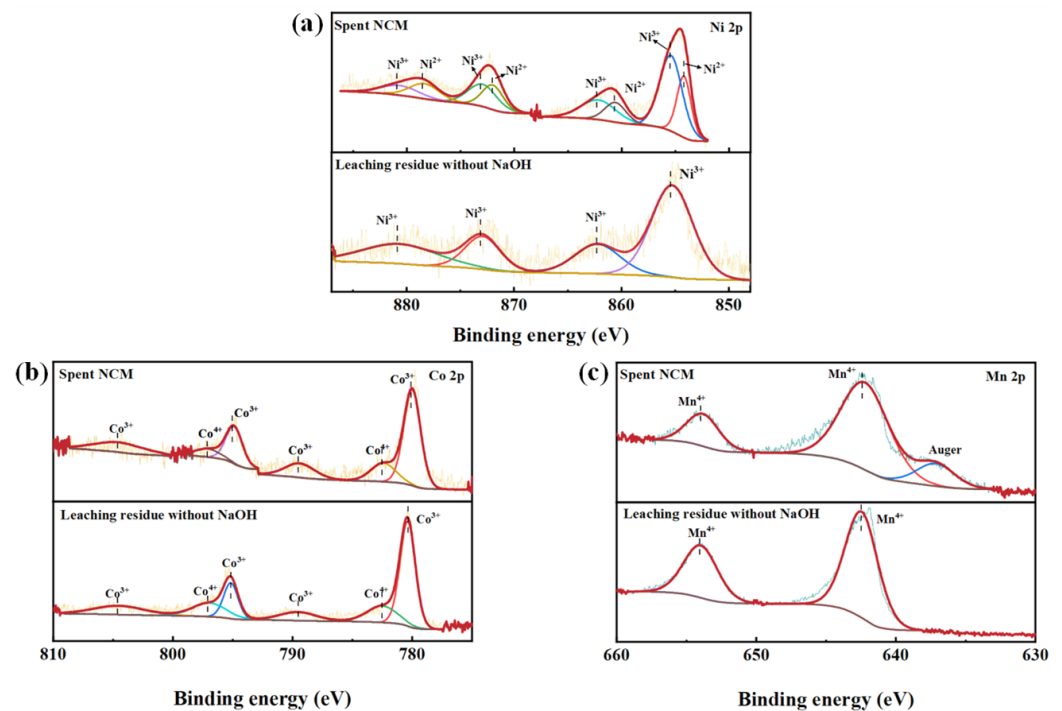
Figure 6. XPS spectra of the samples before and after oxidative leaching (**a**) Ni 2p, (**b**) Co 2p and (**c**) Mn 2p.

The XPS pattern of Co 2p is shown in Figure 6b. There are two main peaks of Co 2p$^{3/2}$ and Co 2p$^{1/2}$ at 780.3 eV and 795.3 eV [34] in the XPS pattern of the spent NCM523 material at the binding energy, and two weaker peaks at 789.3 eV and 804.3 eV at the binding energy belong to Co^{3+}. The two peaks with binding energies of 782.5 eV and 797 eV belong to Co^{4+}. The XPS patterns of Co 2p before and after oxidation acid leaching did not change significantly, indicating that the cobalt remained unchanged in the original structure both before and after leaching, which is also consistent with the minimal amount of cobalt in the leachate. The XPS pattern of Mn 2p is shown in Figure 6c. The binding energy of the spent NCM523 material has two main peaks of Mn 2p$^{3/2}$ and Mn 2p$^{1/2}$ at 642.5 eV and 653.8 eV, which are close to the binding energy data of Mn^{4+} [32,35]. The XPS patterns of Mn 2p did not change significantly from before to after oxidation leaching, indicating that Mn remained unchanged in the original structure both before and after leaching, which is also consistent with the minimal Mn content in the leachate. The XPS patterns before and after the oxidative leaching of the scrap NCM523 can show that the Ni^{2+} in the scrap positive electrode material was partially leached into the solution and partially oxidized to high valence. While both cobalt and manganese were originally maintained at high valence, the leaching retained them in the original structure, and lithium leached into the solution to achieve selective lithium extraction.

3.2. Analysis of Regenerated Materials
3.2.1. Characterization of Regenerated Materials

The XRD patterns of the regenerated material are shown in Figure 7. It can be seen from the figures that the regenerated material was well crystallized and corresponded accurately to the main peaks and PDF cards, indicating the successful preparation of the ternary lamellar material. In general, the ratio of the (003) and (104) diffraction peak intensities can be used to describe the order of the cations. The smaller the ratio of I$_{(003)}$/I$_{(104)}$, the more serious the cation mixing arrangement is. It is generally considered that when I$_{(003)}$/I$_{(104)}$ < 1.2, the Li/Ni mixing of the material is severe. In addition, the value of (I$_{(006)}$ + I$_{(102)}$)/I$_{(101)}$ can represent the degree of order of the crystal structure of the material. In general, a lower value of this ratio indicates a higher degree of order of the crystal struc-

ture. The $I_{(003)}/I_{(104)}$ value of this regenerated material was 2.3 and the $(I_{(006)} + I_{(102)})/I_{(101)}$ value was 1.02, which indicates that the Li/Ni mixing of this material was not serious, and the crystal structure of this material was highly ordered.
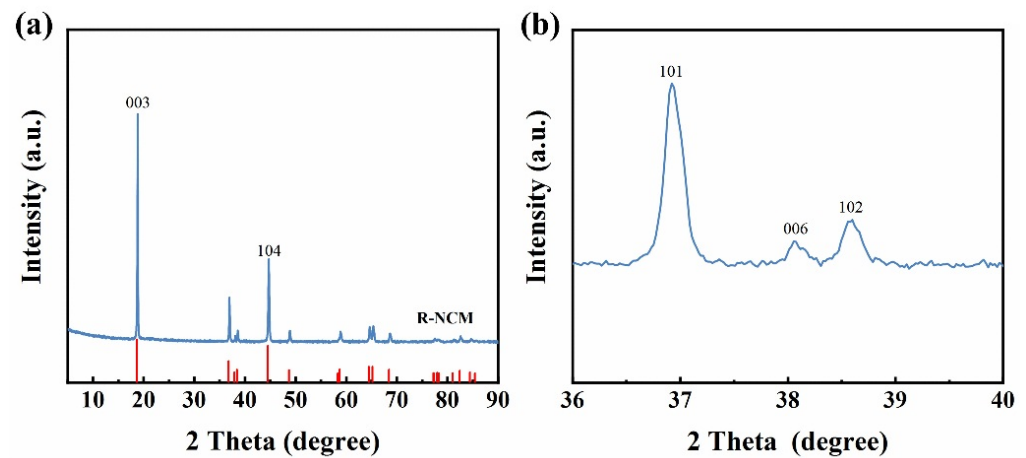

Figure 7. (**a**) XRD pattern of the regenerated material; (**b**) enlarged XRD pattern of the regenerated material.

The microscopic morphology of the regenerated material is shown in Figure 8. Figure 8a–c show the SEM images of the regenerated positive electrode materials, and it can be seen from the figure that the surfaces of the regenerated materials were smooth and the shapes were irregular and sphere-like, but the morphology and particle size had a certain uniformity, and the particle size was 2–3 μm. Figure 8d–i is the mapping image of the material, and it can be observed that the elements such as Ni, Co, Mn, and O were uniformly distributed in the material, which is a prerequisite for the excellent electrochemical properties exhibited by the material.
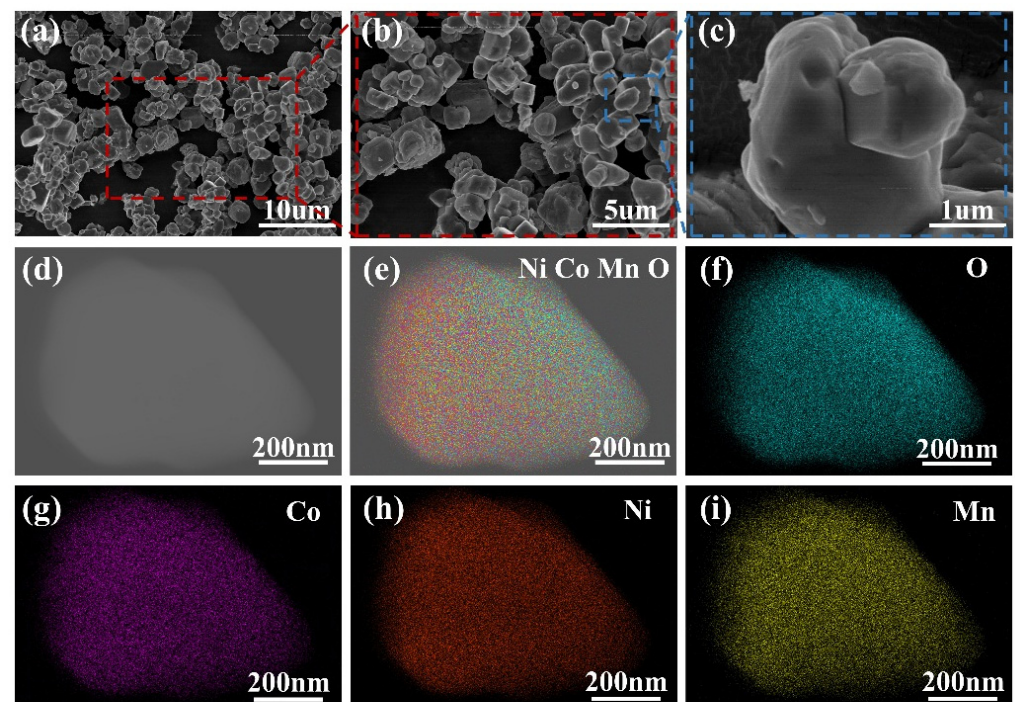
Figure 8. *Cont.*
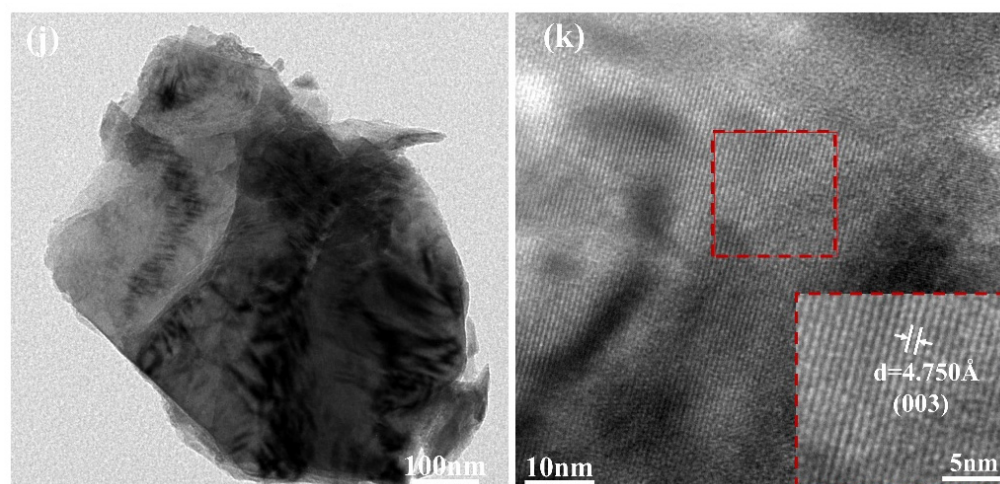
Figure 8. (**a**–**c**) SEM images, (**d**–**i**) Element mapping images, (**j**,**k**) TEM images of regenerated positive electrode material.

The TEM of the regenerated material is shown in Figure 8j,k, and the calculation and comparison of PDF cards yielded that the crystal plane shown is the (003) crystal plane of the *R-3m* space group, which had a spacing d = 4.750 Å. This lattice spacing was slightly larger than the (003) crystal plane spacing of $LiNiO_2$ (d = 0.4746 nm), probably due to the incorporation of Ni and Mn. The larger lattice spacing facilitated the diffusion of Li^+ in the positive electrode lamellar structure.

3.2.2. Analysis of Electrochemical Properties of Regenerated Materials

The electrochemical performance test of the regenerated material is shown in Figure 9. The test environment temperature was 25 °C, the voltage range was 2.8–4.3 V, and the cycle test was conducted at 0.2 C. It can be found from Figure 9a that the charge/discharge capacity of the regenerated material was 181.9/143.2 mAh/g at the first cycle, and the first charge/discharge efficiency was not high, only 78.7%. It is possible that the structure of the regenerated positive electrode material changed after the first discharge due to the delithiation, thus reducing the location of the embeddable lithium in the material, and the lithium ions could not all be embedded back into the positive electrode material during the first discharge. The CVs of the first three circles of the regenerated material are shown in Figure 9b, with a voltage range of 2.8–4.3 V and a scan rate of 0.01 mV/s. It can be seen from the figure that, except for the offset of the first circle, the second and third circles afterwards almost completely overlapped. The offset of the first circle was due to a large interfacial polarization during cycling, which decreased as the cycle proceeded. The test results indicate that the regenerated material had good reversibility during the cycle. The redox peaks on the graph correspond to the redox process of Ni^{2+}/Ni^{4+}, and there are no other peaks other than that, indicating that the material was electrochemically stable in the voltage interval. Figure 9c shows the multiplicity curve of the material, which maintained a capacity of about 150 mAh/g at 0.1 C and 0.2 C. Figure 9d shows the impedance diagram of the material before cycling and the equivalent circuit diagram, and after fitting the material, the ohmic impedance R_1 = 1.4 Ω and the electrochemical reaction impedance R_{ct} = 90.7 Ω. The charging and discharging curves of the regenerated material for 100 cycles are shown in Figure 9e, and the charging and discharging efficiencies of all the cycles were close to 100% except for the first five cycles, which had more side reactions. The discharge capacity of the 100th cycle was 128.9 mAh/g. The capacity retention rate was 90% after 100 cycles, indicating that the material had excellent cycling performance.
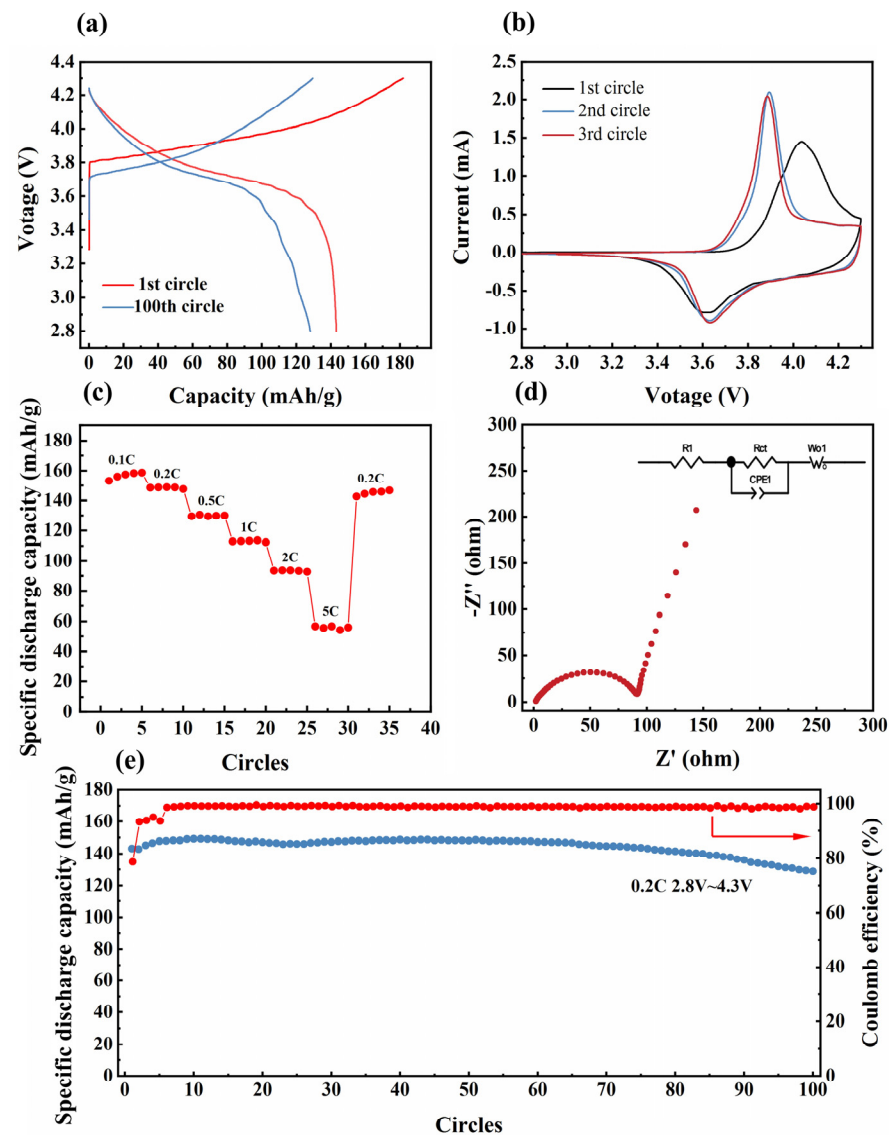
Figure 9. Lithium storage properties. (**a**) Charge/discharge curves of resynthesized positive electrode material, (**b**) CV curves, (**c**) rate capability of resynthesized positive electrode material for different rates, (**d**) Nyquist plots of the samples at open circuit state, (**e**) cycling performances of regenerated positive electrode materials.

4. Conclusions

In this study, the "acid + oxidant" leaching system, which breaks the traditional method, is proposed to achieve selective and efficient leaching of lithium from spent ternary lithium-ion battery positive electrode materials as well as comprehensive utilization of Ni, Co, and Mn resources. In this selective lithium extraction method, the lithium leaching efficiency is as high as 98.7%, and the nickel–cobalt–manganese solids are used as ternary precursors to prepare regenerated positive electrode materials. Electrochemical tests prove that the regenerated material has good electrochemical performance, with a maximum discharge capacity of over 150 mAh/g at 0.2 C rate and a capacity retention rate of over 90% after 100 cycles. This method combines the waste battery recycling process and the material preparation process, providing new ideas for the industrial development of spent LIB recycling.

References

1. D'Andrea, S.; Panero, S.; Reale, P.; Scrosati, B. Advanced lithium ion battery materials. *Ionics* **2000**, *6*, 127–132. [CrossRef]
2. Horiba, T. Lithium-Ion Battery Systems. *Proc. IEEE* **2014**, *102*, 939–950. [CrossRef]
3. Yoshino, A. The Birth of the Lithium-Ion Battery. *Angew. Chem. Int. Ed.* **2012**, *51*, 5798–5800. [CrossRef] [PubMed]
4. Wang, Q.; Mao, B.; Stoliarov, S.I.; Sun, J. A review of lithium ion battery failure mechanisms and fire prevention strategies. *Prog. Energy Combust. Sci.* **2019**, *73*, 95–131. [CrossRef]
5. Zhang, J.-G. Anode-less. *Nat. Energy* **2019**, *4*, 637–638. [CrossRef]
6. Yudha, C.S.; Muzayanha, S.U.; Widiyandari, H.; Iskandar, F.; Sutopo, W.; Purwanto, A. Synthesis of $LiNi_{0.85}Co_{0.14}Al_{0.01}O_2$ Cathode Material and its Performance in an NCA/Graphite Full-Battery. *Energies* **2019**, *12*, 1886. [CrossRef]
7. Barbosa, J.C.; Gonçalves, R.; Costa, C.M.; Lanceros-Mendez, S. Recent Advances on Materials for Lithium-Ion Batteries. *Energies* **2021**, *14*, 3145. [CrossRef]
8. Scrosati, B.; Hassoun, J.; Sun, Y.-K. Lithium-ion batteries. A look into the future. *Energy Environ. Sci.* **2011**, *4*, 3287–3295. [CrossRef]
9. Harper, G.; Sommerville, R.; Kendrick, E.; Driscoll, L.; Slater, P.; Stolkin, R.; Walton, A.; Christensen, P.; Heidrich, O.; Lambert, S.; et al. Recycling lithium-ion batteries from electric vehicles. *Nature* **2019**, *575*, 75–86. [CrossRef]
10. Masias, A.; Marcicki, J.; Paxton, W.A. Opportunities and Challenges of Lithium Ion Batteries in Automotive Applications. *ACS Energy Lett.* **2021**, *6*, 621–630. [CrossRef]
11. Bai, Y.; Muralidharan, N.; Sun, Y.-K.; Passerini, S.; Stanley Whittingham, M.; Belharouak, I. Energy and environmental aspects in recycling lithium-ion batteries: Concept of Battery Identity Global Passport. *Mater. Today* **2020**, *41*, 304–315. [CrossRef]
12. Xu, J.; Cai, X.; Cai, S.; Shao, Y.; Hu, C.; Lu, S.; Ding, S. High-Energy Lithium-Ion Batteries: Recent Progress and a Promising Future in Applications. *Energy Environ. Mater.* **2022**, *6*, e12450. [CrossRef]
13. Dolotko, O.; Hlova, I.Z.; Mudryk, Y.; Gupta, S.; Balema, V.P. Mechanochemical recovery of Co and Li from LCO cathode of lithium-ion battery. *J. Alloys Compd.* **2020**, *824*, 153876. [CrossRef]
14. Wang, M.-M.; Zhang, C.-C.; Zhang, F.-S. Recycling of spent lithium-ion battery with polyvinyl chloride by mechanochemical process. *Waste Manag.* **2017**, *67*, 232–239. [CrossRef] [PubMed]
15. Wang, D.; Zhang, X.; Chen, H.; Sun, J. Separation of Li and Co from the active mass of spent Li-ion batteries by selective sulfating roasting with sodium bisulfate and water leaching. *Miner. Eng.* **2018**, *126*, 128–135. [CrossRef]
16. Liu, P.; Xiao, L.; Tang, Y.; Chen, Y.; Ye, L.; Zhu, Y. Study on the reduction roasting of spent $LiNi_xCo_yMn_zO_2$ lithium-ion battery cathode materials. *J. Therm. Anal. Calorim.* **2018**, *136*, 1323–1332. [CrossRef]
17. Yang, C.; Zhang, J.; Cao, Z.; Jing, Q.; Chen, Y.; Wang, C. Sustainable and Facile Process for Lithium Recovery from Spent $LiNi_xCo_yMn_zO_2$ Cathode Materials via Selective Sulfation with Ammonium Sulfate. *ACS Sustain. Chem. Eng.* **2020**, *8*, 15732–15739. [CrossRef]
18. Fouad, O.A.; Farghaly, F.I.; Bahgat, M. A novel approach for synthesis of nanocrystalline γ-$LiAlO_2$ from spent lithium-ion batteries. *J. Anal. Appl. Pyrolysis* **2007**, *78*, 65–69. [CrossRef]
19. Tan, S.-Y.; Payne, D.J.; Hallett, J.P.; Kelsall, G.H. Developments in electrochemical processes for recycling lead–acid batteries. *Curr. Opin. Electrochem.* **2019**, *16*, 83–89. [CrossRef]
20. Liu, P.; Xiao, L.; Chen, Y.; Tang, Y.; Wu, J.; Chen, H. Recovering valuable metals from $LiNi_xCo_yMn_{1-x-y}O_2$ cathode materials of spent lithium ion batteries via a combination of reduction roasting and stepwise leaching. *J. Alloys Compd.* **2019**, *783*, 743–752. [CrossRef]
21. Liang, J.; Xue, Y.; Gu, J.-N.; Li, J.; Shi, F.; Guo, X.; Guo, M.; Min, X.; Li, K.; Sun, T.; et al. Sustainably recycling spent lithium-ion batteries to prepare magnetically separable cobalt ferrite for catalytic degradation of bisphenol A via peroxymonosulfate activation. *J. Hazard. Mater.* **2021**, *427*, 127910. [CrossRef] [PubMed]
22. Huang, Y.; Han, G.; Liu, J.; Chai, W.; Wang, W.; Yang, S.; Su, S. A stepwise recovery of metals from hybrid cathodes of spent Li-ion batteries with leaching-flotation-precipitation process. *J. Power Sources* **2016**, *325*, 555–564. [CrossRef]
23. Peng, C.; Liu, F.; Wang, Z.; Wilson, B.P.; Lundström, M. Selective extraction of lithium (Li) and preparation of battery grade lithium carbonate (Li_2CO_3) from spent Li-ion batteries in nitrate system. *J. Power Sources* **2019**, *415*, 179–188. [CrossRef]
24. Wang, K.; Zhang, G.; Luo, M.; Zeng, M. Separation of Co and Mn from acetic acid leaching solution of spent lithium-ion battery by Cyanex272. *J. Environ. Chem. Eng.* **2022**, *10*, 108250. [CrossRef]

25. Liang, Z.; Ding, X.; Cai, C.; Peng, G.; Hu, J.; Yang, X.; Chen, S.; Liu, L.; Hou, H.; Liang, S.; et al. Acetate acid and glucose assisted subcritical reaction for metal recovery from spent lithium ion batteries. *J. Clean. Prod.* **2022**, *369*, 133281. [CrossRef]

26. Gu, S.; Kong, J.; Xing, L.; Sun, H.; Qiu, Y.; Yu, J. Insights into the coordination enhanced leaching mechanism of spent lithium-ion batteries cathode materials. *J. Environ. Chem. Eng.* **2022**, *10*, 107745. [CrossRef]

27. Lie, J.; Liu, J.-C. Closed-vessel microwave leaching of valuable metals from spent lithium-ion batteries (LIBs) using dual-function leaching agent: Ascorbic acid. *Sep. Purif. Technol.* **2021**, *266*, 118458. [CrossRef]

28. Ning, P.; Meng, Q.; Dong, P.; Duan, J.; Xu, M.; Lin, Y.; Zhang, Y. Recycling of cathode material from spent lithium ion batteries using an ultrasound-assisted DL-malic acid leaching system. *Waste Manag.* **2019**, *103*, 52–60. [CrossRef] [PubMed]

29. Cheng, X.; Guo, G.; Cheng, Y.; Liu, M.; Ji, J. Effect of Hydrogen Peroxide on the Recovery of Valuable Metals from Spent $LiNi_{0.6}Co_{0.2}Mn_{0.2}O_2$ Batteries. *Energy Technol.* **2022**, *10*, 2200039. [CrossRef]

30. He, L.-P.; Sun, S.-Y.; Mu, Y.-Y.; Song, X.-F.; Yu, J.-G. Recovery of Lithium, Nickel, Cobalt, and Manganese from Spent Lithium-Ion Batteries Using L-Tartaric Acid as a Leachant. *ACS Sustain. Chem. Eng.* **2017**, *5*, 714–721. [CrossRef]

31. Wang, M.; Liu, K.; Yu, J.; Zhang, C.-C.; Zhang, Z.; Tan, Q. Recycling spent lithium-ion batteries using a mechanochemical approach. *Circ. Econ.* **2022**, *1*, 100012. [CrossRef]

32. Yang, C.; Zhang, J.; Yu, B.; Huang, H.; Chen, Y.; Wang, C. Recovery of valuable metals from spent LiNixCoyMnzO$_2$ cathode material via phase transformation and stepwise leaching. *Sep. Purif. Technol.* **2021**, *267*, 118609. [CrossRef]

33. Shaju, K.M.; Subba Rao, G.V.; Chowdari, B.V.R. Performance of layered $Li(Ni_{1/3}Co_{1/3}Mn_{1/3})O_2$ as cathode for Li-ion batteries. *Electrochim. Acta* **2002**, *48*, 145–151. [CrossRef]

34. Zhang, Y.; Wang, W.; Fang, Q.; Xu, S. Improved recovery of valuable metals from spent lithium-ion batteries by efficient reduction roasting and facile acid leaching. *Waste Manag.* **2019**, *102*, 847–855. [CrossRef]

35. Regan, E.; Groutso, T.; Metson, J.B.; Steiner, R.; Ammundsen, B.; Hassell, D.; Pickering, P. Surface and bulk composition of lithium manganese oxides. *Surf. Interface Anal.* **1999**, *27*, 1064–1068. [CrossRef]